



ELSEVIER

Available online at www.sciencedirect.com

SCIENCE @ DIRECT®

Agricultural Water Management 79 (2006) 1–27

Agricultural
water management

www.elsevier.com/locate/agwat

Monitoring wheat phenology and irrigation in Central Morocco: On the use of relationships between evapotranspiration, crops coefficients, leaf area index and remotely-sensed vegetation indices

B. Duchemin^{a,b,*}, R. Hadria^b, S. Erraki^b, G. Boulet^{a,b},
P. Maisongrande^a, A. Chehbouni^{a,b}, R. Escadafal^a, J. Ezzahar^b,
J.C.B. Hoedjes^{a,c}, M.H. Kharrou^d, S. Khabba^b, B. Mougenot^a,
A. Olioso^e, J.-C. Rodriguez^f, V. Simonneaux^{a,b}

^a *Centre d'Etudes Spatiales de la Biosphère (CESBIO), 18 Avenue Edouard Belin,
BPI 2801, 31401 Toulouse Cedex 9, France*

^b *Faculté des Sciences Semlalia (FSS), Avenue Prince My Abdellah, BP 2390, Marrakech 40000, Morocco*

^c *Meteorology and Air Quality Group, Wageningen University, Duivendaal 2,
6701 AP Wageningen, The Netherlands*

^d *ORMVAH, Avenue Hassan II, BP 2411, Marrakech 40000, Morocco*

^e *INRA—Unité Climat, Sol et Environnement, Domaine Saint-Paul, Site Agroparc,
84914 Avignon Cedex 9, France*

^f *IMADES, Reyes y Aguascalientes (esq.), Colonia San Benito, Hermosillo,
Sonora, C.P. 83190, México City, Mexico*

Accepted 18 February 2005

Available online 19 March 2005

Abstract

The monitoring of crop production and irrigation at a regional scale can be based on the use of ecosystem process models and remote sensing data. The former simulate the time courses of the main biophysical variables which affect crop photosynthesis and water consumption at a fine time step (hourly or daily); the latter allows to provide the spatial distribution of these variables over a region of

* Corresponding author. Tel.: +212 44 43 16 26; fax: +212 44 43 16 26.
E-mail address: benoit.duchemin@ird.fr (B. Duchemin).

interest at a time span from 10 days to a month. In this context, this study investigates the feasibility of using the normalised difference vegetation index (NDVI) derived from remote sensing data to provide indirect estimates of: (1) the leaf area index (LAI), which is a key-variable of many crop process models; and (2) crop coefficients, which represent the ratio of actual (AET) to reference (ET_0) evapotranspiration.

A first analysis is performed based on a dataset collected at field in an irrigated area of the Haouz plain (region of Marrakesh, Central Morocco) during the 2002–2003 agricultural season. The seasonal courses of NDVI, LAI, AET and ET_0 have been compared, then crop coefficients have been calculated using a method that allows roughly to separate soil evaporation from plant transpiration. This allows to compute the crop basal coefficient (K_{cb}) restricted to the plant transpiration process. Finally, three relationships have been established. The relationships between LAI and NDVI as well as between LAI and K_{cb} were found both exponential, with associated errors of 30% and 15%, respectively. Because the NDVI saturates at high LAI values (>4), the use of remotely-sensed data results in poor accuracy of LAI estimates for well-developed canopies. However, this inaccuracy was not found critical for transpiration estimates since AET appears limited to ET_0 for well-developed canopies. As a consequence, the relationship between NDVI and K_{cb} was found linear and of good accuracy (15%).

Based on these relationships, maps of LAI and transpiration requirements have been derived from two Landsat7-ETM+ images acquired at the beginning and the middle of the agricultural season. These maps show the space and time variability in crop development and water requirements over a $3 \text{ km} \times 3 \text{ km}$ irrigated area that surrounds the fields of study. They may give an indication on how the water should be distributed over the area of interest in order to improve the efficiency of irrigation. The availability, in the near future, of Earth Observation Systems designed to provide both high spatial resolution (10 m) and frequent revisit (day) would make it feasible to set up such approaches for the operational monitoring of crop phenology and irrigation at a regional scale.

© 2005 Elsevier B.V. All rights reserved.

Keywords: LAI; Leaf area index; Vegetation indices; Wheat; NDVI; Crop coefficients; Evaporation; Transpiration; Evapotranspiration

1. Introduction

This paper presents an experiment on energy and water fluxes of wheat crops as part of the “SudMed” project (Chehbouni et al., 2003, 2004). The overall objective of the project is to understand the processes that affect the water and energy balances of semi-arid areas at the basin scale. The project focuses on South Mediterranean regions with the Tensift river basin (Central Morocco) as a main region of interest. The basin size is about 20,000 km², which includes the Atlas mountain range (headwater) and the semi-arid Haouz plain in the surroundings of the Marrakech city. In the plain, the climate is characterised by low and irregular rainfall with an annual average of about 240 mm, whereas the evaporative demand is very high, around 1600 mm year⁻¹ according to the reference evapotranspiration (ET_0) calculated for well-watered grass following the FAO Penman–Monteith equation (Allen et al., 1998; Allen, 2000). Since rainfall and irrigation are limited hence actual evapotranspiration (AET) is the dominant term of the water balance. Cereals (mainly wheat, also barley) and orchards (mainly citrus and olive trees) are the dominant crop types in the Haouz irrigated areas. This agriculture uses up to 80% of the total available water. Because priority is generally given to orchards in case of water shortage, the actual amount

of water supplied to cereal crops may explain a large part of inter-annual variations of the regional water balance.

In regional water-balance modelling, estimates of AET as well as the partitioning between soil evaporation and plant transpiration are crucial issues, especially in semi-arid regions where scarcity of soil water is an important limiting factor to crop growth and yield. With regard to these issues, the SudMed project focuses on approaches that combine experimental field data, soil–vegetation–atmosphere transfer models, and remote sensing.

Space-borne optical and thermal infrared imagery can be a useful tool to estimate AET at a regional scale (Kite and Droogers, 2000; Schmugge et al., 2002; Courault et al., 2003; Van Niel and McVicar, 2004). A first class of methods has been developed to map instantaneous latent and sensible heat fluxes at the time of satellite overpass only based on remote sensing and climatic data (Brutsaert et al., 1993; Moran et al., 1994; Carlson et al., 1995; Bastiaanssen et al., 1998; McVicar and Jupp, 2002). These approaches show limitations due to the infrequency of observations as a result of cloudiness and orbital schedules.

In contrast, ecosystem process models including water transfer in the soil–vegetation–atmosphere system provide continuous simulations of AET (Lo Seen et al., 1995; Olioso et al., 2003). When linked with remote sensing data, these models provide continuous estimates of the water and energy balances on regular space grid (Moulin et al., 1998; Cayrol et al., 2000; Weiss et al., 2001; Andersen et al., 2002; Clevers et al., 2003). This second class of methods is based on the combination of inversion, calibration and assimilation techniques, which are still difficult to set up and validate in an operational context (Olioso et al., 1999; Jacquemoud et al., 2000; Kimes et al., 2000; François et al., 2001; Combal et al., 2003; Moulin et al., 2003; Verhoef and Bach, 2003; Boegh et al., 2004; Demarty et al., 2004; Mo et al., 2004; Pellenq and Boulet, 2004).

As a third class of methods, there is a room for the improvement of operational tools. Among them, the FAO method has been extensively used to derive AET and to schedule irrigation. It is based on the concepts of reference evapotranspiration (ET_0) and crop coefficients (K_c), which have been introduced to separate the climatic demand from the plant response (e.g. Allen et al., 1998). The reference surface is a well-watered green grass of uniform height and infinite extent, which is actively growing and completely shading the ground. This qualitative description is associated with assumptions on the main biophysical variables of the system: leaf area index (LAI), surface resistance, albedo, canopy height. This allows to define an unambiguous method for calculating ET_0 based on the so-called FAO Penman–Monteith equation (Allen et al., 1998; derived from Penman (1948) and Monteith (1985)). In a second step, the evapotranspiration of a specific crop is obtained by the adjustment of ET_0 using semi-empirical K_c values, which are expected to include all differences in the physio-morphology between the crop in its actual status and the above-described ‘ideal’ grass. For operational application, this approach is often preferred because it only requires phenological and standard meteorological data while providing acceptable AET estimates compared to physically-based modelling and field measurements (Evetts et al., 1995; Allen, 2000; Kite and Droogers, 2000; Eitzinger et al., 2002).

Crop coefficients K_c primarily depend on the dynamics of canopies (cover fraction, LAI, greenness). Since satellite data can help to estimate some key-variables related to

vegetation phenology (e.g. Baret and Guyot, 1991; Hall et al., 1995; Carlson and Ripley, 1997; Myneni et al., 1997; Duchemin et al., 1999; Gutman, 1999; Bastiaanssen et al., 2000), they offer opportunities for monitoring the space and time variability of K_c . Use of remotely-sensed vegetation indices, such as the normalised difference vegetation index (NDVI; Rouse et al., 1974) or the soil-adjusted vegetation index (SAVI; Huete, 1988), has been tested to predict crop coefficients at field and regional scales (Bausch and Neale, 1987; Choudhury et al., 1994; Bausch, 1995; Ray and Dadhwal, 2001; Duchemin et al., 2002).

Local parameterisation of all the above-described methods and models is always required to get accurate AET estimates. Thus, there is a need of field experiments for calibration and validation. The present study is mainly based on a field dataset acquired on irrigated wheat crops during year 2003. Since AET, LAI and NDVI are simultaneously available, the dataset offers an excellent opportunity to test the potential of remote sensing data to infer accurate crops coefficients.

In this context, the objective of this paper is two-fold: (1) to analyse the seasonal dynamics of crop coefficients in response to plant phenology and water availability; and (2) to discuss the potential of vegetation indices derived from satellite data to monitor LAI and AET. The paper is organised as follows. The area of interest and the experiment are presented first, then field data are analysed as follows: LAI is related to NDVI, and their seasonal dynamics are compared to that of actual and reference evapotranspiration; crops coefficients are calculated with a method that allows roughly to separate soil evaporation from plant transpiration. Finally, relationships between the plant transpiration coefficient (K_{cb}), LAI and NDVI are proposed and applied on two Landsat-7/ETM+ satellite images. The results are discussed in the perspective of using remote sensing data as a tool for monitoring the space–time variability of crop phenology and water requirements.

2. Site and experiment overviews

The region of interest is the Haouz plain in the centre of the Tensift basin, Central Morocco, 40 km east of Marrakesh city (Fig. 1). The plain is surrounded by the northern ‘Jbilet’ hills and the southern High-Atlas mountain range. The High-Atlas culminates up to 4000 m above sea at the Toubkal summit, the highest of North Africa. The Atlas range is indeed the region’s water bank, supplying several big irrigated areas in the plain (Chaponnière et al., *in press*).

The experiment took place in one of the irrigated areas (located in Fig. 1), which has been managed since 1999 by a regional public agency (Office Régional de Mise en Valeur Agricole du Haouz (ORMVAH)). In Fig. 2, this area is presented on a very high spatial resolution image acquired by the Quickbird satellite (Meek et al., 2002). The area covers 2800 ha and is practically flat. The main land cover class is cereals, mostly wheat then barley. The fields are generally sown between November 15 and January 15, and the harvest occurs after 5–6 months, in May or June. The dominant soil-type is xerosol (FAO classification), developed on colluvial materials from the High-Atlas mountain range. This results in homogeneous deep soils (generally more than 1 m) with a fine, clay to loamy, texture. Consequences for soil water characteristics are a very low hydraulic conductivity

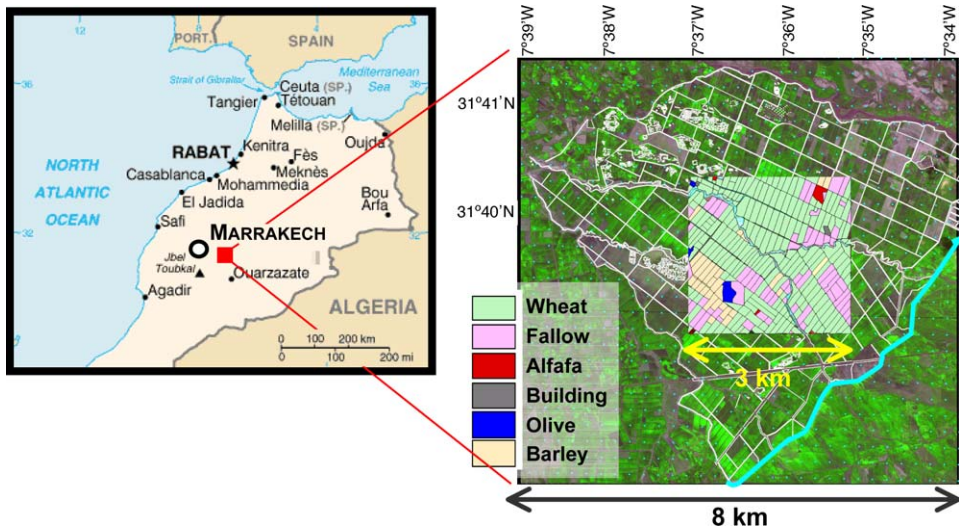


Fig. 1. Location of the experiment: on the left, the general map of Morocco highlights the Marrakech city (blank circle) and the experimental site (red square); on the right, the whole irrigated area is delineated on a Quickbird multispectral image (2.4 m resolution), along with the irrigation units (white lines), the main channel (cyan curve) and the land cover (coloured shapes) during the 2002–2003 agricultural season.

and a large soil water capacity for plants. Shallow calcareous crusts of less than 1 m in depth are limited to local patches.

In this irrigated area, ORMVAH, together with three local farmer associations, is in charge of the dam water distribution. At the beginning of the agricultural campaign, they decide the periods for several irrigation rounds, which are regularly distributed from December to May. The number of rounds (0–6) and the global amount of water per round (generally less than 60 mm in equivalent-water depth) depend on the dam water levels. The amount per farm is simply calculated as a linear function of the farm total area; it does not vary with season, crop type and status. However, the farmers can decide to fallow a part of their fields in order to have more water in the cropped part or to transfer it to adjacent farms. Ground water may also be used for irrigation. The number of wells has considerably increased during the last few years, from around 40 in 2001 to more than 60 in 2004. As a consequence, the water table is dropping, between 30 and 50 m nowadays. Ground water is used in priority for orchards, forages (alfalfa) and vegetables, but can also be used for cereal in case of high shortage of dam water. This general scheme results in a large heterogeneity in the water supply in terms of amount and periods of distribution.

The experiment was set up at the beginning of the 2002–2003 wheat agricultural season. Three irrigation rounds were decided on by ORMVAH, with an amount of around 30 mm in equivalent-water depth each time. Rainfall was close to normal, with a cumulated value of around 250 mm between December and May and a bimodal distribution: one peak occurred before mid-December and the other after mid-March, but very few rain were observed between these dates. A supplementary irrigation round was decided on at the end of the season since the dams were filled by large precipitations in Spring (an accumulated

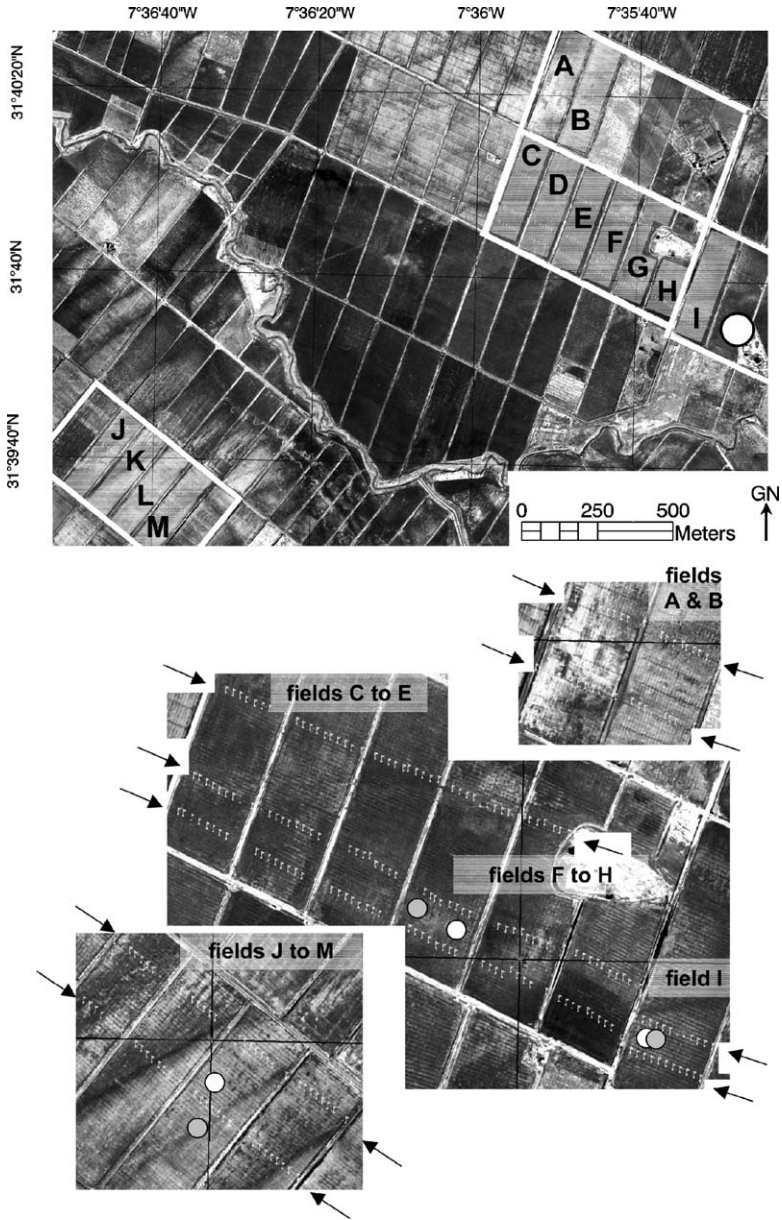


Fig. 2. Description of the experimental site as seen by Quickbird in the panchromatic mode (60 cm resolution). In the top figure, the 13 fields of study are labelled with letters ('A' to 'M' from north to south), the surrounding irrigation units are highlighted (white rectangles) and the meteorological station is located (white disk). Zoomed areas in the bottom figure show the places of: (1) the towers equipped with evapotranspiration measurement systems (grey disks), net radiation sensors and soil heat flux plates (white disks); (2) the transects sampled with the hand-held radiometer (white flags between black arrows correspond each to one plot where surface reflectances have been recorded).

Table 1
Set of biophysical variables measured during the experiment

Variable	Location	Temporal basis	Spatial scale	Method
Leaf area index	All fields	Month	0.5–1.25 m ²	Metric observation
Canopy reflectance	All fields ^a	Week	≈40 m ²	Hand-held radiometer
Climatic forcing	Close to field I ^b	Half-hour	Few km ²	Meteorological sensors
Latent heat flux	Fields F, I and L ^b	Half-hour	100 m ² to few ha	Eddy correlation systems

^a The records are made along the transects visible in areas zoomed in Fig. 2.

^b The towers and pits where these measurements are collected are located in Fig. 2.

value of around 130 mm was observed between March 16 and April 19 in the area). Each irrigation round takes about 3 weeks, during which time the whole area is supplied through a system of concrete channels that supplies the water from the main channel to regular irrigation units (Figs. 1 and 2). Each unit consists on average of six fields of 4 ha where the agricultural practices (sowing, irrigation, fertilisation) are usually homogeneous. Flood irrigation technique is used.

From January to May 2003, the experiment was carried out on wheat crops to monitor the variables of the surface energy and water balances during plant growth, maturity and senescence. In March 2003, the land cover was recorded field-by-field on a 3 km × 3 km square centred on the irrigated area: wheat was generally dominant and represented around 60% of this 9 km² area (Fig. 1). We studied 13 fields within 4 irrigation units (labelled from A to M in Fig. 2). Clay dominates in the deep soils of all these fields. The set of biophysical variables obtained during the experiment is summarised in Table 1 and detailed further.

3. The experimental dataset

3.1. Leaf area index

On each of the 13 fields and every 3 weeks, we have estimated the area of green leaves per area of soil from metric and phenological observations. At regular intervals, two to five small square “plots” (i.e. elementary area of 0.25 m² = 0.5 m × 0.5 m) were sampled. On each plot, the leaf density was derived from the plant density and the average number of green leaves per plant. In a second step, five plants were selected at random to measure the size of each leaf, i.e. the length (L) and width (W) of a rectangle that encompasses the leaf. The average leaf area was estimated as the product of the mean leaf size ($L \times W$) and a reduction coefficient that depends of the leaf shape (0.87 for wheat after Owen (1968) and Ledent (1976)). The average leaf area was multiplied by the leaf density to calculate the LAI on each plot. The minimum, maximum and average values over the different plots were finally computed.

3.2. Normalised difference vegetation index

We used a hand-held MSR87 multispectral radiometer (Cropscan Inc., USA). This instrument measures both incoming and reflected radiation over eight optical spectral

bands including the six ones of Thematic Mapper (TM) sensors onboard the successive Landsat missions. Two of these bands are centred on red (0.63–0.69 μm) and near-infrared (0.76–0.90 μm) wavelengths. The NDVI is defined as the difference between near-infrared and red reflectances divided by their sum (Rouse et al., 1974).

On a weekly basis, surface reflectances were collected along several transects every 10 m. Wood markers were installed in the fields to allow the observations to be made at the same place from one date to another (blank flags in the areas zoomed in Fig. 2). Each measurement was taken holding the MSR87 sensor 3 m high in a vertical position. The field-of-view being 28° , the instrument samples each time an elementary area of around 2 m^2 . According to the size of the field and the number of sampled transects, 10–30 observations were collected per field at a particular date. The average and the standard deviation of NDVI were computed, field-by-field, from these elementary measurements.

3.3. LAI and NDVI at field scale

Flood irrigation is used on the experimental site through a mosaic of rows located within the fields. These rows results in a fine linear spatial texture that can be observed on a Quickbird image, as it can be easily seen for fields D and I in areas zoomed in Fig. 2. They are spaced on average every 5 m and their size is around 1 m. They represent 20% of the fields, which have not been sampled during LAI measurements since the plant density is almost null. Therefore, we reduced the values obtained from the field measurements by a factor of 20% to upscale the LAI from plot to field values.

Using the very high spatial resolution of Quickbird data (2.4 m in multispectral mode), we have assessed the spatial consistency of NDVI between transects and fields. Digital counts associated to red and near-infrared channels were converted in luminances then in top-of-atmosphere reflectances following Krause (2003). Finally a top-of-atmosphere NDVI image was built. For each field, two plots of interest were drawn on the image: the first just encompassed the transects (around 0.1 ha) while the second recovered the entire field (about 3 ha). NDVI statistical moments were extracted for each of these plots of interest and compared to each other, as well as to the values obtained at surface using the MSR87 radiometer. Only the data collected on the 20th and 28th of March, i.e. close to the image acquisition date (March 25, 2003), were used for this comparison.

The result of the comparison is displayed in Fig. 3. The NDVI derived from the Quickbird values are similar at both transect and field scales (Fig. 3, left). We conclude that the sample of MSR87 observations was sufficient to consider the transect values as representative of field ones. The offset in the mean values between the MSR87 surface reflectance and Quickbird top-of-atmosphere reflectance remains constant from one field to another (Fig. 3, right). MSR87 and Quickbird NDVI measurements differ, since: (1) the spectral bands do not match exactly; (2) the time of acquisition and the sun–target–sensor geometry were not the same; and (3) the atmospheric effects on reflectances can be strong (Rahman, 1996). The offset is in the range of values found in previous comparative studies: average differences of 0.1 between surface and top-of-atmosphere NDVI for both SPOT-1 HRV and Landsat-5 TM sensors, and differences ranging from 0.01 to 0.05 in surface NDVI between these two sensors (Guyot and Gu, 1994); shift of up to 0.2 in top-of-

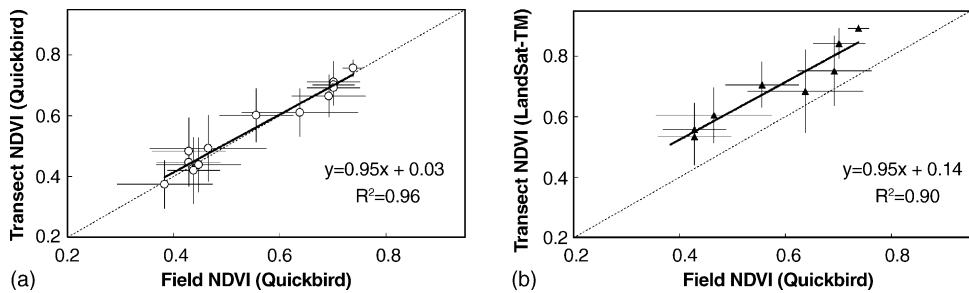


Fig. 3. NDVI derived on the 13 fields from the multispectral Quickbird image (March 25, 2003) and the hand-held MSR87 radiometer (March 20 and 28, 2003, only eight fields were sampled at these two dates). Figure on left allow to compare transect- and field-averaged top-of-atmosphere values derived from the Quickbird image. Figure on right displays the same comparison but with transect values collected at surface using the MSR87 radiometer. Horizontal and vertical bars show the NDVI standard deviation within fields and transects, respectively.

atmosphere NDVI for NOAA-11 AVHRR due to change in the illumination conditions of the target (Privette et al., 1995).

Vertical bars in Fig. 3 also show how large the heterogeneity of canopies is. When considering the Quickbird values at field scale, the NDVI averages range from 0.3 to 0.7 with standard deviation between 0.03 and 0.11. This heterogeneity was visible on very high spatial scale resolution imagery, particularly for fields A, H and K in the areas zoomed in Fig. 2.

3.4. Latent heat fluxes

Latent heat fluxes were collected using three 2 m towers at the places indicated by blank disks in Fig. 2 (bottom). The towers were equipped with eddy covariance instruments which have provided high frequency (10 Hz) measurements of turbulent structures: three-dimensional (3D) air velocity and temperature were measured using two systems of sonic anemometers (CSAT3, Campbell Scientific Inc., USA and Ultrasonic Anemometer Model 81000, R.M. Young Company, USA); synchronous water vapour concentration measurements were done at two of the three sites using fast hygrometers (LI-7500, Li-Cor Inc., USA and KH2O, Campbell Scientific Inc., USA). Surface net radiation and soil heat flux were recorded on additional towers (grey disks in Fig. 2) at half-hour intervals. The experimental set-up in the area was as follows:

- *Field F*: CSAT3 and CO₂/H₂O gas analyser (LI-7500) from days 35 to 140, with a lack of data at the beginning of the season due to problems with the power supply. A CR5000 datalogger (Campbell Scientific Inc., USA) was used for the storage of raw 10 Hz data.
- *Field I*: Young 81000, net radiation (Q7, Campbell Scientific Inc., USA) and soil heat flux plates (HFP3 plates, REBS Inc., USA), from days 78 to 128. Raw 10 Hz data of the 3D ultrasonic anemometer were stored on a portable computer using the program Tourbillon v. 1.0, which has been developed at the Institut National de la Recherche Agronomique (INRA), Bioclimatology Section, Bordeaux, France. No fast humidity measurements were available.

- *Field L*: Same system as field I from days 65 to 70, then CSAT3 sonic anemometer and KH2O krypton hygrometer from days 73 to 148. The data were processed directly online; the half-hourly fluxes were stored on a CR23X datalogger (Campbell Scientific Inc., USA).

At fields F and I, an eddy covariance analysis was carried out on the raw 10 Hz data to calculate the sensible heat fluxes (using the average of the covariance between vertical wind speed and temperature fluctuations) and the latent heat fluxes (using the average of the covariance between vertical wind speed and humidity fluctuations). This calculation was performed for half-hour intervals using the post-processing EdiRe software package. The software used for the processing of the raw data is available for download from <http://www.geos.ed.ac.uk/abs/research/micromet/EdiRe/Downloads.html>. In the processing coordinate rotations are carried out on the measurements of the 3D sonic anemometers, the sonic temperature is corrected for the lateral velocity and the presence of humidity, frequency response corrections are made for slow apparatus and path length integration, and the mean vertical velocity according to Webb et al. (1980) is included.

Finally, the half-hourly average values of the latent heat fluxes were accumulated to obtain daily values of the actual evapotranspiration (in mm).

3.5. Reference evapotranspiration and crop coefficients

The use of reference evapotranspiration (ET_0) derived from different surfaces with different methods (De Bruin and Stricker, 2000; Wright et al., 2000; Kashyap and Panda, 2001; Kassam and Smith, 2001; Eitzinger et al., 2002) may lead to a lack of consistency between estimates of crop water requirements. The FAO has reached agreement in recommending the Penman–Monteith equation—with the parameterisation as elaborated by Allen et al. (1998)—as the best performing method to estimate reference evapotranspiration (Walter et al., 2000). This method was adopted here (Eq. (1)):

$$ET_0 = \frac{0.408\Delta(R_n - G) + \gamma(900/(T + 273))u_2(e_s - e_a)}{\Delta + \gamma(1 + 0.34u_2)} \quad (1)$$

(after Allen et al., 1998)

where ET_0 is the reference evapotranspiration at 2 m height (mm day^{-1}); R_n is the net radiation at the crop surface ($\text{MJ m}^{-2} \text{day}^{-1}$); G is the soil heat flux density ($\text{MJ m}^{-2} \text{day}^{-1}$); T is the daily average of air temperature ($^{\circ}\text{C}$); u_2 is the wind speed (m s^{-1}); e_s and e_a are the saturation and actual vapour pressure (kPa), respectively; Δ is the slope of the vapour pressure curve ($\text{kPa } ^{\circ}\text{C}^{-1}$); and γ is the psychrometric constant ($\text{kPa } ^{\circ}\text{C}^{-1}$).

Climatic data were recorded very close to the fields of interest (blank disk in Fig. 2, top) at two heights (2 and 6 m) using a tower equipped with classical automatic sensors: incoming solar radiation (CNR1, Kipp & Zonen, The Netherlands), air temperature and vapour pressure (HMP45C, Vaisala, Finland), wind speed (A100R anemometer, R.M. Young Company, USA), rainfall (FSS500 tipping bucket automatic rain gauge, Campbell Inc., USA). The meteorological station was installed on December 17, 2002. Data included half-hourly measurements of incoming solar radiation, wind speed, air temperature and

humidity. Using averages or sums, daily values were calculated in order to compute ET_0 at 2 m height through the FAO Penman–Monteith equation (Eq. (1)), strictly following the screening and correction recommended by Allen et al. (1998).

According to this calculation, the cumulated value of ET_0 was around 550 mm during the 2003 agricultural season (December–May). This represented up to twice the rainfall accumulated during the same period. Actual crop coefficients (K_{c_act}) were finally calculated as the ratio of AET to ET_0 (Eq. (2)). As shown by Eq. (3), K_{c_act} can be expressed as a combination of three coefficients (K_e , K_{cb} and K_s) to account for soil evaporation, plant transpiration and water stress, respectively:

$$AET = K_{c_act} \times ET_0 \quad (2)$$

$$K_{c_act} = K_s \times K_{cb} + K_e \quad (\text{after Allen, 2000}) \quad (3)$$

where K_{c_act} and K_{cb} are the actual and basal crop coefficients, K_e is a soil evaporation coefficient and K_s is the stress reduction coefficient.

4. LAI–NDVI relationship

Fig. 4 presents the time courses of NDVI and LAI for one field per irrigation unit (see Fig. 2, keeping in mind that a field is rather representative of the others in the same unit).

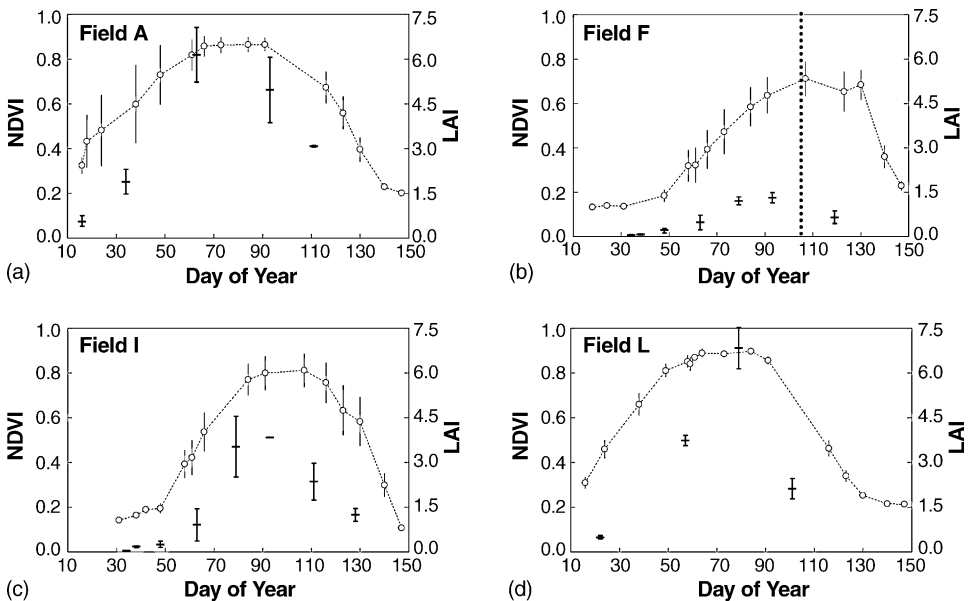


Fig. 4. LAI (–) and NDVI (○) seasonal dynamics of wheat crops in the four irrigation units: (a) field A, with sowing date (SD) around December 23, 2002; (b) field F, SD \approx January 10, 2003; (c) field I, SD \approx January 15, 2003; (d) field L, SD \approx December 17, 2002. Bars in time series indicates standard deviation in the case of NDVI and extreme (minimal and maximal) values in the case of LAI. The vertical dotted line in (b) indicates the start of growing of a wild oat over wheat in field F.

The two variables exhibit comparable seasonal patterns, primarily following the dynamics of the density and greenness of leaves. Fields A, I and L display high values of LAI (>4) and NDVI (>0.8), which indicate acceptable growth conditions (Fig. 4a, c and d). The NDVI curves flat out at mid-season with reduced standard deviation as the NDVI saturates for high values of LAI, when the soil was almost totally covered by the canopy. On field F (Fig. 4b), plant growth was delayed and reduced at the beginning of the season, whereas a wild oat invaded the field after mid-April. The contrast between high NDVI and low LAI at the end of the season is due to the fact that NDVI measurements were taken on a mixture of oat and wheat while the LAI was only recorded on wheat plants. No satisfactory reason has been found to explain the lack of growth in field F and the surrounding fields in the same irrigation unit (C–H; see Fig. 2). The possible explanations lie on soil hardness, superficial ploughing and absence of fertilisation during the growing phase. It is also probable that fields C to H have suffered from water stress because of an inadequate irrigation scheduling. Indeed, rainfall were limited (80 mm, with no event larger than 15 mm) and only one irrigation event (30 mm) from mid-December to mid-March. Under these specific conditions, it is thus not obvious to quantify the correlation between NDVI and LAI from Fig. 4.

Since LAI direct destructive measurements were very time-consuming, they were done on very small elementary plots (0.5 m²) and only few plots were sampled, most of the time 2 at full coverage. The heterogeneity of canopies then resulted in large differences between minimal and maximal LAI values, with inconsistency in time (see the vertical bars in Fig. 4, comparing, for instance, days 93 and 111 (field A) or days 79 and 93 (field I)).

In order to obtain a clear relationship, we have compared the observations of the 13 fields together, with NDVI values linearly interpolated at the dates of LAI acquisition. In most of cases, this interpolation was not necessary since the two variables were collected the same day. After this processing, the NDVI shows a logarithmic response to LAI (Fig. 5), in agreement with the results obtained in previous studies (Asrar et al., 1984; Baret

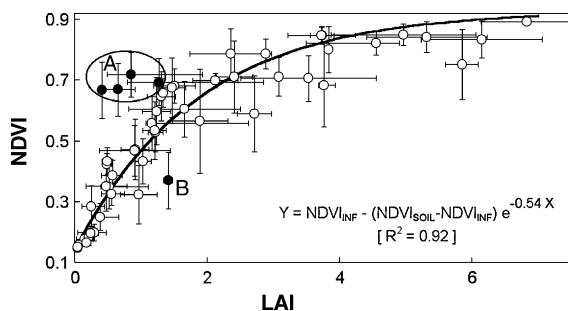


Fig. 5. LAI–NDVI relationship. Symbols are centred on field-averaged LAI and NDVI values. Horizontal bars display the minimal and maximal LAI values observed. Vertical bars show the NDVI standard deviations. An exponential relationship is fit on the scatterplot with infinitely-dense canopy ($NDVI_{INF} = 0.93$) and soil ($NDVI_{SOIL} = 0.14$) values adjusted according to specific observation. The black symbols highlight some points that have been eliminated before the fit: zone A includes the measurements taken on a mixture of oat and wheat (irrigation unit of field F after April; see Figs. 2 and 4b); the point B is obtained with a doubtful interpolation of NDVI (a period of 25 days separates the measurements).

et al., 1989; Richardson et al., 1992). The comparison clearly shows the NDVI saturation at high LAI values. The relationship is tight at low range (LAI from 0 to 1.5), scattered at medium range (LAI from 1.5 to 4), thereafter the variables no longer correlate (LAI > 4). Assuming a linear relationship within each of these three intervals, a regression analysis leads to correlation coefficients of 0.95, 0.64, 0.26 and slopes of 0.35, 0.08 and 0.01 for low, medium and large ranges, respectively. These statistics confirms the lack of sensitivity of NDVI at high LAI values.

Finally, an exponential relationship was fit on the LAI–NDVI scatterplot (Fig. 5) based on two extreme values: $NDVI_{INF}$ is believed to correspond to an infinitely-dense canopy and was defined at 0.93 after looking at maximum values taken on individual plots (flags in Fig. 2); $NDVI_{SOIL}$ has been fixed equal to 0.14 around the minimum value that was observed for dry bare soils at the beginning of the season. The use of the exponential equation derived in Fig. 5 is associated to the following statistics: no bias, correlation coefficient of 0.96, relative error of 30%. The highest accuracy was observed during the initial growing and the end of senescence stages (the root mean square errors associated to Fig. 5 is 0.3 when LAI is lower than 2 against 0.75 when all the values are kept). The surface sampled on NDVI time series was of large spatial extent compared to the direct metric measurements of LAI (see Table 1). Inverting the relationship found in Fig. 5 thus allows us to obtain frequent LAI estimates with an acceptable space sampling. These estimates are used in the following parts of this study.

5. Seasonal trends in evapotranspiration, LAI and NDVI

The seasonal courses of leaf area index, actual and reference evapotranspirations are plotted together in Fig. 6. The LAI was obtained from NDVI using the equation derived in Fig. 5. ET_0 ranges between 2 and 5 mm day⁻¹, then reaches 6–8 mm at the end of May (field L—days 130–150) since there was a regional rise in both air temperature and water vapour deficit, which was locally reinforced by the decrease in evapotranspiration due to the drying of soil.

AET was generally close to ET_0 as soon as the LAI is greater than 2, from the mid-growing to the end-of-maturity period (Fig. 6). At the same time, the daily variation of AET and ET_0 were highly correlated, except during two periods: after day 128 for field F (Fig. 6a), and from days 87 to 100 for field L (Fig. 6c). Since these periods occurred a long time after irrigation, we can assume that plants have suffered from water stress. The absence of correlation between AET and ET_0 is due to the fact that soil water availability is reduced during these two periods.

The correlation between AET and ET_0 also strongly decreased outside of the periods of vegetation growing and maturity (Fig. 6a and c). In this case, low vegetation cover may result in large soil evaporation, depending on top-soil water availability. Although few data were available at the beginning of the season, this can be clearly seen by comparing the three first periods of valid measurements on field F (Fig. 6a):

- (1) After the first irrigation (day 35), AET and ET_0 were comparable during a short time (days 36–40), then AET decreases while ET_0 stays at the same level (days 41–43).

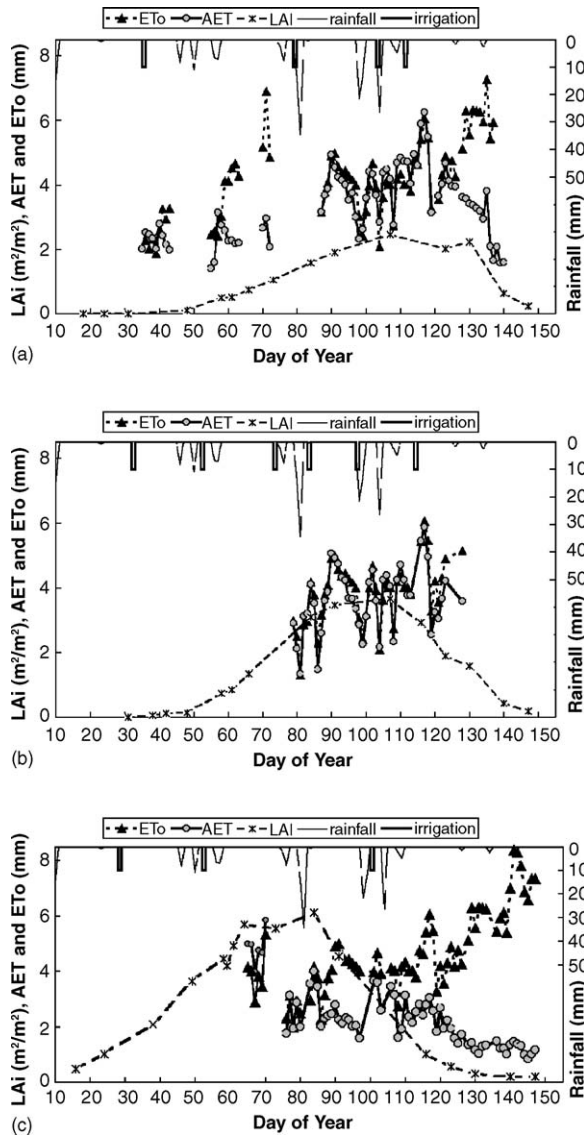


Fig. 6. Seasonal dynamics of leaf area index (LAI, stars on dashed lines), actual (AET, grey disks on solid lines) and reference (ET_0 , black triangles on dotted lines) evapotranspirations, along with water supply events (daily rainfall and irrigation dates). Values on fields F, I and L are displayed in (a), (b) and (c), respectively.

- (2) After a rainfall event of low intensity (around 7 mm during days 56 and 57), AET immediately drops, even though ET_0 increases (days 57–63).
- (3) When no water supply occurred for a long time (this guarantees low soil evaporation), AET may be correlated to ET_0 because of plant transpiration, with a ratio that depends on LAI, e.g. 0.5 when LAI worth 1 (days 70–72).

Fig. 7 displays the seasonal courses of NDVI along with the ratio of actual to reference evapotranspiration (AET/ET₀). This ratio represents the actual crop coefficient (K_{c_act}) that was introduced in Eq. (2); it measures both plant transpiration and soil evaporation and varies according to canopies status and soil water availability. Our comments are three-fold:

- When NDVI is high and the vegetation is unstressed, the ratio of AET on ET₀ is on average 1 and can reach 1.2 (Fig. 7). It should be notice than AET can be larger than ET₀, which is defined for a short canopy (well-watered grass, see Section 1). The range of variation of maximal values for K_{c_act} is consistent with other values found in the literature for highly-covering vegetation (e.g. Allen, 2000; Kang et al., 2003). Differences between studies lie in the difficulty to measure AET and to estimate ET₀ from climatic data acquired in environments that do not strictly match the definition of the reference surface.
- K_{c_act} drops rapidly during stress events (field F—after day 128 in Fig. 7a; field L—after day 87 in Fig. 7c), while the NDVI may still be high and stable during some days after the beginning of water stress (at least until days 130 and 91 for fields F and L, respectively). The water shortage does not affect considerably and immediately neither the capacity of canopies to absorb photosynthetically active radiation nor the structural properties of the plant. As the NDVI saturates, this index is not a good instantaneous indicator of plant water stress (Moran et al., 1994).
- Because of peaks in evaporation after irrigation or rain events and sensitivity of reflectances to the soil top-layer wetness, NDVI and K_{c_act} are not well correlated at the beginning of the season (Fig. 7a before day 72). The correlation is higher at the end of the season (Fig. 7c after day 100) since the vegetation, even senescent, is limiting soil evaporation.

6. Relationships between NDVI, LAI and basal crop coefficient

LAI and NDVI values were interpolated at a daily time step to be compared with continuous series of K_{c_act} for the entire growing season. The result of the comparison is displayed in Figs. 8 and 9. There is a lot of scatter since: (1) AET is the sum of soil evaporation and plant transpiration under various conditions (i.e. dry or wet top-soil, sparse or dense canopies, well-watered or stressed plants); (2) the surface was heterogeneous and the exact area subjected to AET measurements (i.e. the footprint of the eddy covariance systems) may vary from one day to the next, according to stability, wind speed and direction. These figures first confirm that under the prevailing conditions, there is no obvious link between the evapotranspiration and the canopy status as described by the LAI or NDVI variables.

Black symbols in Figs. 8 and 9 highlight the data selected according to the two following criteria: (1) no water supply was observed during a given period (4 days in case of rain and 10 days in case of irrigation), in order to reduce the influence of soil evaporation; (2) stress events were eliminated based on the lack of correlation between AET and ET₀ (after day 128 for field F, days 87–100 for field L; see Fig. 6a and c), in order to raise transpiration at a maximal rate. This processing resulted in the elimination of two groups of points: the first one, with high K_{c_act} versus low LAI and NDVI values,

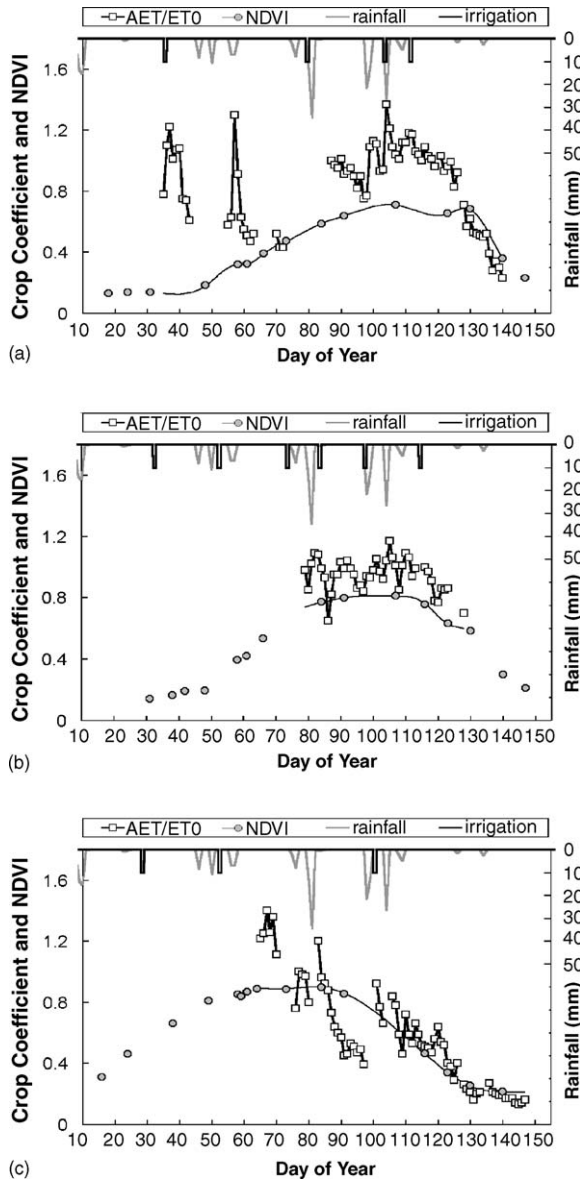


Fig. 7. Seasonal dynamics of NDVI (grey disks) and actual crop coefficient ($K_{c_act} = AET/ET_0$, blank squares), along with water supply events (daily rainfall and irrigation dates). Values on fields F, I and L are displayed in (a), (b) and (c), respectively. NDVI is cubically interpolated during the period of AET measurement.

corresponds to the periods where soil evaporation was predominant; the second one, with low K_{c_act} versus high LAI and NDVI values, was associated to the stress events not captured by the NDVI. The remaining data are thus believed to be acquired on well-watered plants ($K_s \rightarrow 1$ in Eq. (3)) with very low soil evaporation ($K_e \rightarrow 0$ in Eq. (3)).

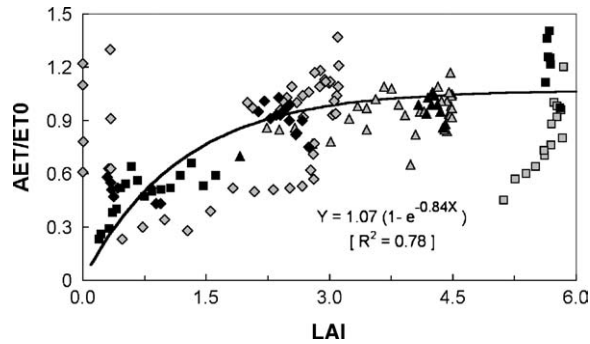


Fig. 8. LAI– K_c relationship. Crop coefficients (K_c) are computed as the ratio of actual and reference evapotranspiration (AET/ET_0) on the Y-axis. Values for fields F (diamonds), I (triangles) and L (squares) are presented together. Black symbols highlight the data for which soil evaporation is reduced and plant transpires at full rate: they allow to approximate crop basal coefficients ($K_c = K_{cb}$) using an exponential relationship.

Under these conditions, Eq. (2) allows to estimate maximal transpiration and K_{c_act} matches the definition of the crop basal coefficient (K_{cb} in Eq. (3)).

After this selection, the relationships between LAI, NDVI and K_{cb} clearly appear, with correlation coefficient around 0.9 (R in Figs. 8 and 9). As in Allen et al. (1998), K_{cb} appears exponentially related to LAI, even if some values are surprisingly high for low-covering vegetation (LAI < 0.7 in Fig. 8). The exponential relationship underestimate these values, which are probably affected by some residual soil evaporation. It is important to note that the NDVI–LAI and K_{cb} –LAI relationships look similar (compare Figs. 5 and 8). This means that both plant transpiration and light absorption increase roughly at the same rate at the beginning of the season, then saturates. As a first consequence, a loss of accuracy in the estimate of high LAI due to NDVI saturation will have little impact on the accuracy of transpiration estimates. As a second consequence, the relationship between NDVI and K_{cb}

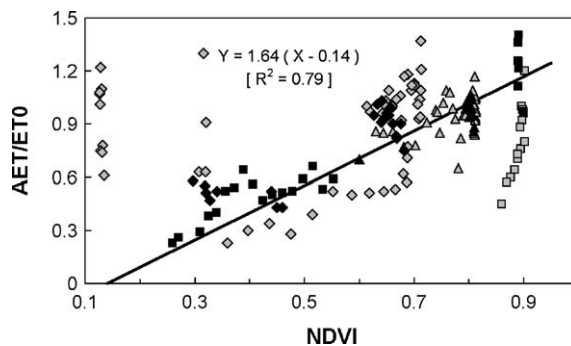


Fig. 9. NDVI– K_c relationship. Crop coefficients (K_c) are computed as the ratio of actual and reference evapotranspiration (AET/ET_0) on Y-axis. Values for fields F (diamonds), I (triangles) and L (squares) are presented together. Black symbols highlight the data for which soil evaporation is reduced and plant transpires at full rate: they allow to approximate crop basal coefficients ($K_c = K_{cb}$) using a linear relationship. The relationship has been forced to include the soil point (NDVI = 0.14; $K_{cb} = 0$).

is linear (Fig. 9), with the same underestimation of K_{cb} for low NDVI values (<0.4). Statistics associated to the estimate of K_{cb} from LAI and NDVI through the equations derived in Figs. 8 and 9 are of the same range (root mean square around 0.14, mean relative error around 16%). These values are comparable to previous works on wheat crops, but the parameters of equations may slightly differ due to inconsistency in the vegetation indices (SAVI in the case of Ray and Dadwhal (2001)), the reference evapotranspiration (Priestley–Taylor formula in Choudhury et al. (1994), pan evaporation method in Bandyopadhyay and Mallick (2003)), and the definition of crop coefficients (K_{cb} in Choudhury et al. (1994); $K_c = K_{cb} + K_e$ in Ray and Dadwhal (2001) as well as in Bandyopadhyay and Mallick (2003); K_{cb} and K_c in Kang et al. (2003)).

7. Spatial estimates of LAI and transpiration requirements

During the 2003 season, a time series of high spatial resolution images have been acquired by the SPOT and Landsat satellites over the Marrakech plain. In order to illustrate the potential of such data for the monitoring of crop phenology and irrigation, we used two Landsat7-ETM+ images that were acquired for contrasted conditions, at the beginning and at the middle of the agricultural season (January 23 and March 31, 2003, respectively).

7.1. Processing of Landsat7-ETM+ images

The images were geometrically corrected using GPS ground control points. The radiometric processing (calibration and atmospheric correction) was performed based on the surface NDVI values that were recorded at field using the MSR 87 hand-held radiometer (see Fig. 2). For this comparison, we first calibrated the ETM+ images to obtain top-of-atmosphere reflectances from digital counts (using the calibration coefficients provided with the images), then we calculated top-of-atmosphere NDVI on some selected areas where surface NDVI was available close to the time of the Landsat overpasses. Reliable linear relationships were found by comparing top-of-atmosphere and surface measurements (Fig. 10) and applied in order to obtain surface NDVI images. However, it should be noticed that the NDVI range is limited to low values for the first date (January 23), since the crops have just begun to grow (sowing dates between December 15 and January 15 for the fields of study).

This pre-processing is justified since effects of both calibration and atmospheric correction on NDVI are nearly linear (Guyot and Gu, 1994; Dinguirard and Slater, 1999; Rao and Chen, 1999). Moreover, it guarantees the consistency between field and satellite observations. Thus, the relationships found between field-NDVI and either LAI or K_{cb} can be confidently applied on images, provided that the land cover class is wheat. The whole processing is summarised below:

- (1) Surface NDVI images were extracted on the $3 \text{ km} \times 3 \text{ km}$ square at the centre of the area of interest.
- (2) A binary mask (wheat or other classes) was built from the land cover map (see Fig. 1).
- (3) This mask was superimposed on surface NDVI images to keep only wheat pixels.

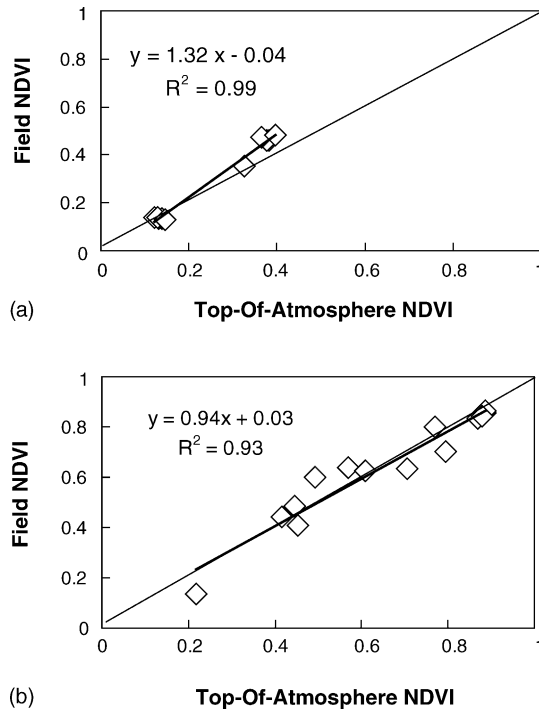


Fig. 10. Comparison of field-averaged NDVI values collected at surface with the MSR87 radiometer and recorded by Landsat-ETM+ sensor on 23th of January (a) and 31th of March (b), 2003.

- (4) Minimal and maximal thresholds were applied on NDVI (0.14, the soil value, and 0.92, corresponding to a maximal LAI value of around 8; see Fig. 5).
- (5) Maps of LAI and K_{cb} were calculated on a pixel basis applying the equations displayed in Figs. 5 and 9.
- (6) Maps of transpiration requirements were obtained by multiplying K_{cb} by ET_0 , which was 2.9 and 4.9 mm on the 23th of January and 31th of March, respectively.

It is important to well understand what is the meaning of transpiration requirement. Indeed, for a given NDVI value, the range of plant transpiration can be very large depending on soil moisture (see Fig. 9). Consequently, optical remote sensing data does not allow to directly estimate actual transpiration but a maximal value that would be observed if water is readily available in the soil. We have referred this maximal value to as transpiration requirement.

7.2. Maps of LAI and transpiration requirements

Figs. 11 and 12 display the results of the above-described processing. The contrast between the two dates is obvious. At the beginning of the season (end of January), LAI was generally low, with an average value of 0.75. End of March is generally the period with the

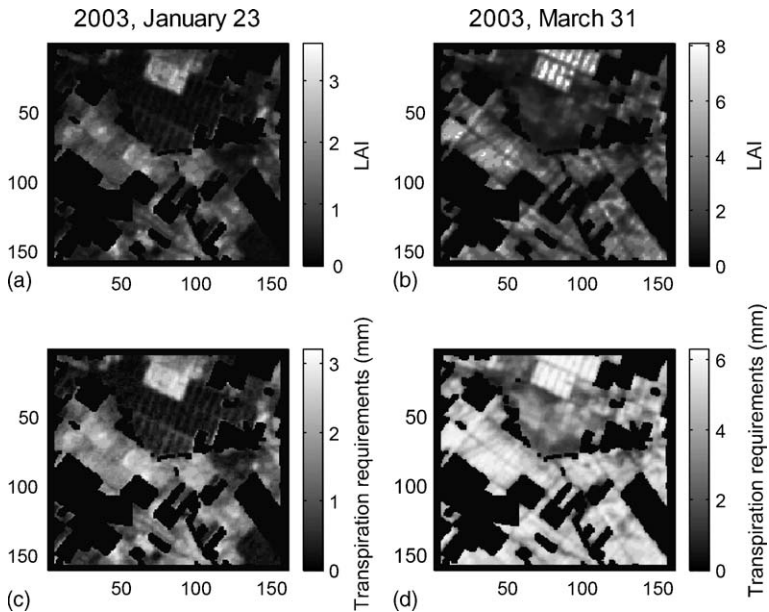


Fig. 11. The $3\text{ km} \times 3\text{ km}$ maps of LAI (a and b) and transpiration requirements (c and d) derived for wheat fields on the centre of the irrigated area from Landsat7-ETM+ images acquired on 23th of January (a and c) and 31th of March (b and d), 2003. The colour bars range level the minimal to the maximal LAI values using a linear grey scale. Pixels that are always black correspond to land cover classes different than wheat (see Fig. 1).

peak of green aerial biomass in the area of interest; the LAI reached on average 2.4 at this time, and the maximum estimated values of around 8 were unrealistic (see the histograms in Fig. 12a and b). These unrealistically high values are a consequence of the saturation effect we discussed from Fig. 5: small uncertainty on NDVI at high values, associated to the radiometric processing of the images, may result in a large overestimation of LAI.

The area appears also very heterogeneous in terms of crop phenological status; LAI standard deviations calculated from the entire images were 80% and 60% of the average value in January and March, respectively. Keeping in mind the spatial organisation of the fields (see Fig. 1), inter- and intra-field variability caused by changes of environment (e.g. soil characteristics) and agricultural practices (e.g. sowing dates, irrigation) can be seen on the images (Fig. 11a and b). The histogram was bimodal in January (Fig. 12a), with the first mode near zero associated to the most recent sowing dates. This trend was smoothed in March near the peak of LAI.

Maps of transpiration requirements appear a little more regular (Fig. 11c and d), especially at the middle of the season (Fig. 11d). The average value was 1.14 mm in January, with a high standard deviation (66% of the average value). This high spatial variability came from differences in sowing dates, resulting in two peaks in the histograms (Fig. 12a and c). Transpiration requirements were raised by a factor of up to 3.5 at end of March (average value was 4.17 mm), because both LAI and ET_0 considerably increased. At

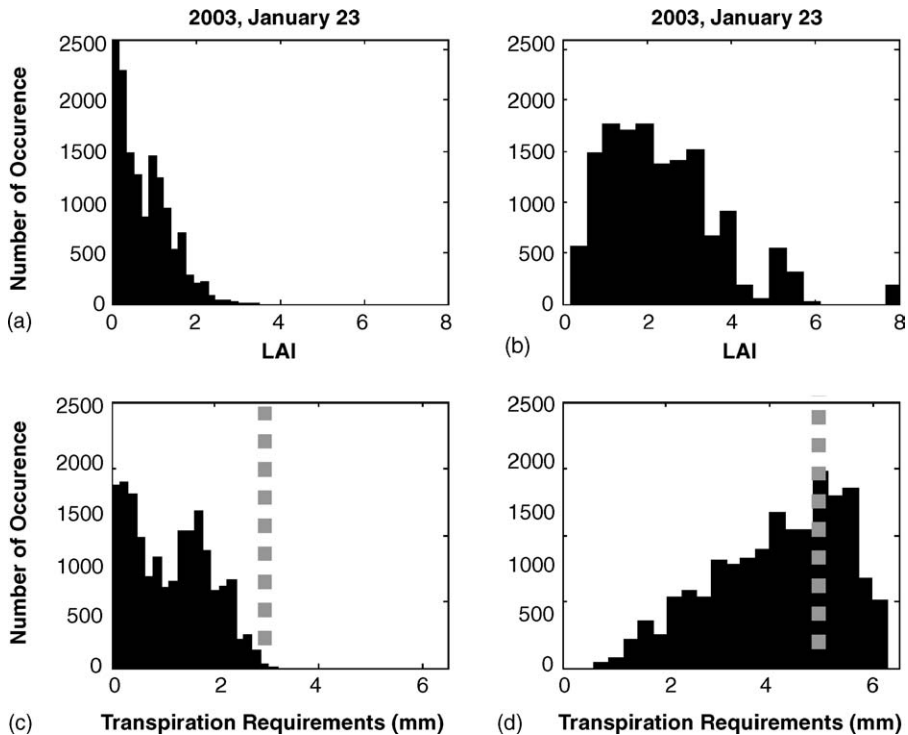


Fig. 12. Histograms associated to the maps of LAI (a and b) and transpiration requirements (c and d) which are displayed in Fig. 11. The values of reference evapotranspiration (ET_0) are highlighted by vertical grey dotted lines; it is 2.9 mm the January 23, 2003 (a and c) and 4.9 mm the March 31, 2003 (b and d).

this date, the patterns of the histograms were different for these two variables (compare Fig. 12b and d): LAI was centred on a median value around 2 with some very high values (above-discussed artefacts), while transpiration requirements shifted near the maximum values since the basal crop coefficient K_{cb} saturates for LAI values larger than 2 (see Fig. 8). This explains the limited spatial variation of transpiration requirements (standard deviation around 30% of the average value).

8. Conclusion

The monitoring of crop production and irrigation at a regional scale can be based on the use of ecosystem process models and remote sensing data. The former simulate the temporal dynamics of the biophysical variables which affect crop photosynthesis and water consumption at a fine time step (hourly or daily); the latter allows to provide the spatial distribution of these variables over a region of interest at a time span of 10 days to a month. This explains the growing interest in developing methods to use remotely-sensed information in ecosystem process models (Olioso et al., 1999; Jacquemoud et al., 2000;

Kimes et al., 2000; François et al., 2001; Van Niel and McVicar, 2002; Combal et al., 2003; Moulin et al., 2003; Verhoef and Bach, 2003; Boegh et al., 2004; Demarty et al., 2004; McVicar et al., 2004; Mo et al., 2004; Olioso et al., in press; Pellenq and Boulet, 2004). However, operational applications have often been hampered by the inability to provide a spatial distribution of the complete set of variables and parameters required by the models. In this context, we have investigated the feasibility of using the normalised difference vegetation index derived from satellite data to provide indirect estimates of leaf area index and crop coefficients. The LAI is a key-variable of ecosystem process models and soil–vegetation–atmosphere transfer models. The crop coefficients can be combined with climatic data to compute evapotranspiration, a dominant term of the water balance in semi-arid areas.

Our analysis was primarily based on a dataset collected at field in an irrigated area of the Haouz plain (region of Marrakesh, Central Morocco) during the 2002–2003 agricultural season. The experimental protocol allows the availability of LAI and NDVI on 13 wheat fields. Amongst them, three fields were equipped with a system to measure AET, while a meteorological station located in the vicinity was used to calculate ET_0 . Using simple criteria applied on LAI and water supply (dates of irrigation and rainfall), the periods where either soil evaporation or plant transpiration dominates were separated. Water-stress periods were located by looking at the correlation between AET and ET_0 . This allows us to establish the relationships between LAI, NDVI and basal crop coefficients ($K_{cb} = AET/ET_0$, when soil evaporation is reduced and plant transpires at a full rate), at a field scale and on a daily basis.

The relationship between LAI and NDVI was found exponential. Based on this relationship, inversion of LAI from satellite data would provide estimates with an associated error of 30%, provided the land cover is known and the radiometry is consistent with that of the hand-held radiometer we used in this study. This relationship can be very useful to couple modelling and remote sensing approaches through forcing, calibration or assimilation procedures. However, due to saturation, the use of NDVI for the estimation of LAI results in poor accuracy for well-developed canopies. When LAI reaches a threshold ranging from 2 to 6 depending on the vegetation type, the addition of more leaves in canopies is not captured by NDVI (Baret and Guyot, 1991; Hall et al., 1995). This threshold was around 4 for wheat according to this study.

The relationships found between LAI or NDVI and K_{cb} were of better accuracy (relative error of 16%). The first relationship between LAI and K_{cb} was found exponential. It can be introduced into soil–vegetation–atmosphere transfer models. Indeed, these models generally derive actual evapotranspiration by calculating first a maximal evapotranspiration as the sum of soil potential evaporation and plant transpiration requirements, before reducing it depending on soil water availability. Based on this relationship, transpiration requirements can be derived from daily LAI and ET_0 time series. The second relationship between NDVI and K_{cb} was found linear. It may help in developing simple and operational methods to monitor crop water requirements using a time series of images, in complement with approximations or estimates of soil evaporation. According to this relationship, NDVI time series can be translated in transpiration requirements with only standard meteorological data required. When the number of observations is limited, interpolations can be performed based on simple models that simulate crop phenology, aerial biomass and

LAI from climatic data (e.g. Weir et al., 1984; Maas, 1993). The availability, in a near future, of Earth Observation Systems designed to provide both high spatial resolution and frequent time of revisit—such as RHEA (Dedieu et al., 2003) or ROCSAT (Chern et al., 2001)—should make it possible to set up such approaches for the operational monitoring of irrigation at a regional scale.

It is important to note that K_{cb} as well as NDVI saturates at large LAI values. Consequently, transpiration requirements can be confidently derived using satellite data: large inaccuracy in LAI derived from NDVI, which may be observed for well-developed canopies, will result in smaller error in estimates of transpiration requirements. In contrast, it is important to fit reliable relationships when the vegetation is partially covering the soil, i.e. at the beginning of the growth.

The features of the area of interest (fields of large extent, flat topography, wheat as the dominant crop) made it very well adapted to test the suitability of remote sensing for the monitoring of crop phenology and irrigation. As a first application, 9 km × 9 km maps of LAI and transpiration requirements were processed from two Landsat7-ETM+ images acquired on the 23th of January and 31th of March, 2003. The maps provide with an indication on how the water should be distributed spatially and temporally in order to improve the efficiency of irrigation. Because of both low LAI and ET_0 values, the transpiration requirements were found low at the first date, with a space average of 1.17 mm and a high spatial variability (66% of the average value). Since both LAI and ET_0 values increased at the second date, the transpiration requirements were found much higher, with a space average of 4.17 mm and a reduced spatial variability (30% of the average value). These maps illustrate the potential of high spatial resolution imagery for providing space–time estimates of biophysical variables required to monitor the water balance of irrigated areas.

Acknowledgements

This study was funded by the European Commission through two 5th Framework INCO-MED programs: WATERMED (WATER use Efficiency in natural vegetation and agricultural areas by Remote sensing in the MEDITerranean basin, <http://www.uv.es/ucg/watermed>) and IRRIMED (“Improved management tools for water-limited irrigation: combining ground and satellite information through models”, <http://www.irrimed.org/>). French CNRS-PNTS (‘Programme National de Télédétection Spatiale’ by ‘Centre National de Recherche Scientifique’, see <http://www.insu.cnrs.fr/web/article/programmes.php>) and CNES-ISIS (‘Incitation à l’utilisation Scientifique des Images SPOT’ by ‘Centre National d’Etudes Spatiales’, see <http://medias.obs-mip.fr/isis>) programs are acknowledged for their support. The authors are very grateful to the following persons for their scientific and technical helps: A. Abourrida, A. Cheggour, S. Errouane, N. Guemouria, A. Lahrouni and A. Lakhal (FSS); G. Dedieu, P. Gentine and D. Helson (CESBIO); J.-M. Bonnefond, M. Irvine and O. Marloie (INRA); I.K. Cherkaoui, L. Ouzine, A. Qabbaj and A. Ramadi (ORMVAH); H. de Bruin and O. Hartogensis (Wageningen University). During a part of this study, J.C.B. Hoedjes was supported by a fellowship from STW, The Netherlands (project no. WMO3544).

References

- Allen, R.G., Pereira, L.S., Raes, D., Smith, M., 1998. Crop evapotranspiration: guidelines for computing crop water requirements. FAO Irrigation and Drainage Paper 56, Rome, 300 pp.
- Allen, R.G., 2000. Using the FAO-56 dual crop coefficient method over an irrigated region as part of an evapotranspiration intercomparison study. *J. Hydrol.* 229, 27–41.
- Andersen, J., Dybkjaer, G., Jensen, K.H., Refsgaard, J.C., Rasmussen, K., 2002. Use of remotely sensed precipitation and leaf area index in a distributed hydrological model. *J. Hydrol.* 264 (1–4), 34–50.
- Asrar, G., Fuchs, M., Kanemasu, E.T., Hatfield, J.L., 1984. Estimating absorbed photosynthetic radiation and leaf area index from spectral reflectance in wheat. *Agron. J.* 76, 300–306.
- Bandyopadhyay, P.K., Mallick, S., 2003. Actual evapotranspiration and crop coefficients of wheat (*Triticum aestivum*) under varying moisture levels of humid tropical canal command area. *Agric. Water Manage.* 59, 33–47.
- Baret, F., Guyot, G., Major, D.J., 1989. Crop biomass evaluation using radiometric measurements. *Photogrammetria* 43, 241–256.
- Baret, F., Guyot, G., 1991. Potentials and limits of vegetation indices for LAI and APAR assessment. *Remote Sens. Environ.* 35, 161–173.
- Bastiaanssen, W.G.M., Menenti, M., Feddes, R.A., Holtslag, A.A.M., 1998. A remote sensing surface energy balance algorithm for land (SEBAL): I. Formulation. *J. Hydrol.* 212–213 (1–4), 198–212.
- Bastiaanssen, W.G.M., Molden, D.J., Makin, I.W., 2000. Remote sensing for irrigated agriculture: examples from research and possible applications. *Agric. Water Manage.* 46 (2), 137–155.
- Bausch, W.C., Neale, C.M.U., 1987. Crop coefficient derived from reflected canopy radiation: a concept. *Trans. ASAE* 30 (3), 703–709.
- Bausch, W.C., 1995. Remote sensing of crop coefficients for improving the irrigation scheduling of corn. *Agric. Water Manage.* 27, 55–68.
- Boegh, E., Thorsen, M., Butts, M.B., Hansena, S., Christiansen, J.S., Abrahamsen, P., Hasager, C.B., Jensen, N.O., Van der Keur, P., Refsgaard, J.C., Schelde, K., Soegaard, H., Thomsen, A., 2004. Incorporating remote sensing data in physically based distributed agro-hydrological modelling. *J. Hydrol.* 287 (1–4), 279–299.
- Brutsaert, W., Hsu, A.Y., Schmugge, T.J., 1993. Parameterization of surface heat fluxes above forest with satellite thermal sensing and boundary layer soundings. *J. Appl. Meteorol.* 32, 909–917.
- Carlson, T.N., Capehart, W.J., Gillies, R.R., 1995. A new look at the simplified method for remote sensing of daily evapotranspiration. *Remote Sens. Environ.* 54, 161–167.
- Carlson, T.N., Ripley, D.A., 1997. On the relation between NDVI, vegetation cover and leaf area index. *Remote Sens. Environ.* 62, 241–252.
- Cayrol, P., Chehbouni, A., Kergoat, L., Dedieu, G., Mordelet, P., Nouvellon, Y., 2000. Grassland modeling and monitoring with SPOT-4 vegetation. *Agric. For. Meteorol.* 105, 91–115.
- Chaponnière, A., Maisongrande, P., Duchemin, B., Hanich, L., Boulet, G., Escadafal, R., Elouaddat, S. A combined high and low spatial resolution approach for mapping snow covered area in the atlas mountain. *Int. J. Remote Sens.*, in press.
- Chebouni, A., Escadafal, R., Dedieu, G., Errouane, S., Boulet, G., Duchemin, B., Mougnot, B., Sminonneaux, V., Seghieri, J., Timouk, F., 2003. A multidisciplinary program for assessing the sustainability of water resources in semi-arid basin in Morocco: SUDMED. In: Proceedings of the EGS–AGU–EUG Joint Assembly, Nice, France, 6–11 April.
- Chebouni, A., Escadafal, R., Boulet, G., Duchemin, B., Dedieu, G., Hannich, L., et al., 2004. Integrated modelling and remote sensing approach for sustainable management of water resources in Tensift region (SudMed): preliminary results, current status and new challenges. In: Proceedings of the International Conference on Integrated Water Resources Research and Development in Southeastern Morocco, Ouarzazate, Morocco, 1–2 April.
- Chern, J.-S., Lee, L.-C., Wang, H.-C., Chu, F.-H., 2001. An introduction to NSPO and ROCSATs missions. In: Proceedings of the Third IAA Symposium on Small Satellites for Earth Observation, Berlin, Germany, 2–6 April.
- Choudhury, B.J., Ahmed, N.U., Idso, S.B., Reginato, R.J., Daughtry, C.S.T., 1994. Relations between evaporation coefficients and vegetation indices studied by model simulations. *Remote Sens. Environ.* 50, 1–17.

- Clevers, J.G.P.W., Vonder, O.W., Jonschaap, R.E., Desprats, J.F., King, C., Bruguier, L., Prévot, N., 2003. Using Spot data for calibrating a wheat growth model under Mediterranean conditions. *Agronomie* 22, 687–694.
- Combal, B., Baret, F., Weiss, M., Trubuil, A., Macé, D., Pragnère, A., Myneni, R., Knyazikhin, Y., Wang, L., 2003. Retrieval of canopy biophysical variables from bidirectional reflectance: using prior information to solve the ill-posed inverse problem. *Remote Sens. Environ.* 84 (1), 1–15.
- Courault, D., Seguin, B., Olioso, O., 2003. Review to estimate evapotranspiration from remote sensing data: some examples from the simplified relationship to the use of atmospheric models. In: *ICID Workshop on Remote Sensing of ET for Large Regions*, Montpellier, France, 17 September.
- De Bruin, H.A.R., Stricker, J.N.M., 2000. Evaporation of grass under non-restricted soil moisture conditions. *Hydrol. Sci.* 45, 391–406.
- Dedieu, G., Cabot, F., Chehbouni, A., Duchemin, B., Maisongrande, P., Boulet, G., Pellenq, J., 2003. RHEA: a micro-satellite mission for the study and modeling of land surfaces through assimilation techniques. In: *Proceedings of the EGS–AGU–EUG Joint Assembly*, Nice, France, 6–11 April.
- Demarty, J., Ottle, C., Braud, I., Olioso, A., Frangi, J.P., Bastidas, L.A., Gupta, H.V., 2004. Using a multiobjective approach to retrieve information on surface properties used in a SVAT model. *J. Hydrol.* 287 (1–4), 214–236.
- Dingirard, M., Slater, P.N., 1999. Calibration of spatial-multispectral imaging sensors: a review. *Remote Sens. Environ.* 68, 194–205.
- Duchemin, B., Goubier, J., Courrier, G., 1999. Monitoring phenological key-stages and cycle duration of temperate deciduous forest ecosystems with NOAA-AVHRR data. *Remote Sens. Environ.* 67, 51–67.
- Duchemin, B., Frappart, F., Maisongrande, P., Magnac, M., Mougénot, B., Chehbouni, A., Dedieu, G., 2002. Water budget with phenology derived from optical satellite data. In: *Proceedings of the First International Symposium of Recent Advances in Quantitative Remote Sensing*, Valencia, Spain, 16–20 September.
- Eitzinger, J., Marinkovic, D., Hösch, J., 2002. Sensitivity of different evapotranspiration calculation methods in different crop-weather models. In: Rizzoli, A.E., Jakeman, A.J. (Eds.), *Integrated Assessment and Decision Support. Proceedings of the First Biennial Meeting of the International Environmental Modelling and Software Society (IEMSS)*, vol. 2, Lugano, Switzerland, 24–27 June, pp. 395–400.
- Evert, S.R., Howell, T.A., Schneider, A.D., Tolk, J.A., 1995. Crop coefficient based evapotranspiration estimates compared with mechanistic model results. In: Espey, W.H., Combs, P.G. (Eds.), *Water Resources Engineering. Proceedings of the First International Conference*, vol. 2, San Antonio, TX, USA, 14–18 August.
- François, C., Cayrol, P., Kergoat, L., Moulin, S., Dedieu, G., 2001. Assimilation techniques of remote sensing measurements into vegetation models: overview, limits and promises. In: *Proceedings of the Eighth Symposium on Physical Measurements and Signatures in Remote Sensing of International Society for Photogrammetry and Remote Sensing (ISPRS)*, Aussois, France, 8–12 January.
- Gutman, G.G., 1999. On the use of long-term global data of land reflectances and vegetation indices derived from the advanced very high resolution radiometer. *J. Geophys. Res.* 104, 6241–6255.
- Guyot, G., Gu, X.-F., 1994. Effect of radiometric correction on NDVI-determined from SPOT-HRV and Landsat-TM data. *Remote Sens. Environ.* 49, 169–180.
- Hall, F.G., Townshend, J.R., Engmann, E.T., 1995. Status of remote sensing algorithms for estimation of land surface parameters. *Remote Sens. Environ.* 51, 138–156.
- Huete, A.R., 1988. A soil-adjusted vegetation index (SAVI). *Remote Sens. Environ.* 25, 295–309.
- Jacquemoud, S., Bacour, C., Poilvé, H., Frangi, J.-P., 2000. Comparison of four radiative transfer models to simulate plant canopies reflectance: direct and inverse mode. *Remote Sens. Environ.* 74 (3), 471–481.
- Kang, S., Gu, B., Du, T., Zhang, J., 2003. Crop coefficient and ratio of transpiration to evapotranspiration of winter wheat and maize in a semi-humid region. *Agric. For. Meteorol.* 59, 239–254.
- Kashyap, P.S., Panda, R.K., 2001. Evaluation of evapotranspiration methods and development of crop-coefficients for potato crop in a sub-humid region. *Agric. Water Manage.* 50, 9–25.
- Kassam, A., Smith, M., 2001. FAO methodologies on crop water use and crop water productivity. In: *Proceedings of the Expert Meeting on Crop Water Productivity*, Rome, Italy, 3–5 December.
- Kimes, D.S., Knyazikhin, Y., Privette, J.L., Abuelgasim, A.A., Gao, F., 2000. Inversion methods for physically-based models. *Remote Sens. Rev.* 18, 381–439.
- Kite, G.W., Droogers, P., 2000. Comparing evapotranspiration estimates from satellites, hydrological models and field data. *J. Hydrol.* 209, 3–18.

- Krause, K., 2003. Radiance Conversion of QuickBird Data. RS_TN_radiometric_radiance_4002 technical note available at <http://www.digitalglobe.com/>.
- Ledent, J.-F., 1976. Beam light interception by twisted leaf surfaces. *Agric. Meteorol.* 17, 271–280.
- Lo Seen, D., Mougin, E., Rambal, S., Gaston, A., Hiernaux, P., 1995. A regional Sahelian grassland model to be coupled with multispectral satellite data: II. Toward the control of its simulation by remotely sensed indices. *Remote Sens. Environ.* 52, 194–206.
- Maas, S.J., 1993. Parameterized model of gramineous crop growth: I. Leaf area and dry mass simulation. *Agron. J.* 85, 348–353.
- McVicar, T.R., Jupp, D.L.B., 2002. Using covariates to spatially interpolate moisture availability in the Murray–Darling basin: a novel use of remotely sensed data. *Remote Sens. Environ.* 79, 199–212.
- Meek, M., Gold, K., Hwang, Y., Axelrad, P., Born, G., 2002. Orbit determination for the Quickbird spacecraft. In: *Proceedings of the Core Technologies for Space Systems Conference*, Colorado Springs, CO, USA, 19–21 November.
- Mo, X., Liu, S., Lin, Z., Zhao, W., 2004. Simulating temporal and spatial variation of evapotranspiration over the Lushi basin. *J. Hydrol.* 285 (1–4), 125–142.
- Monteith, J.L., 1985. Evaporation from land surfaces: progress in analysis and prediction since 1948. In: *Proceedings of the ASAE Conference on Evapotranspiration*. Chicago, ILASAE, St. Joseph, Michigan.
- Moran, M.S., Clarke, T.R., Inoue, Y., Vidal, A., 1994. Estimating crop water deficit using the relation between surface–air temperature and spectral vegetation index. *Remote Sens. Environ.* 49, 246–263.
- Moulin, S., Bondeau, A., Delécolle, R., 1998. Combining agricultural crop models and satellite observations from field to regional scales. *Int. J. Remote Sens.* 19, 1021–1036.
- Moulin, S., Kergoat, L., Cayrol, P., Dedieu, G., Prévot, L., 2003. Calibration of a coupled canopy functioning and SVAT model in the ReSeDA experiment: Towards the assimilation of SPOT/HRV observations into the model. *Agronomie* 22, 681–686.
- Myneni, R.B., Keeling, C.D., Tucker, C.J., Asrar, G., Nemani, R.R., 1997. Increased plant growth in the northern high latitudes 1981 to 1991. *Nature* 386, 698–702.
- Oliosio, A., Chauki, H., Courault, D., Wigneron, J.P., 1999. Estimation of evapotranspiration and photosynthesis by assimilation of remote sensing data into SVAT models. *Remote Sens. Environ.* 68 (3), 341–356.
- Oliosio, A., Braud, I., Chanzy, A., Courault, D., Demarty, J., Kergoat, L., Lewan, E., Otlé, C., Prévot, L., Zhao, W.G., Calvet, J.-Ch., Cayrol, P., Jongschaap, R., Moulin, S., Noilhan, J., Wigneron, J.P., 2003. SVAT modeling over the Alpes-ReSeDA experiment: comparing SVAT models over wheat fields. *Agronomie* 22, 651–668.
- Oliosio, A., Inoue, Y., Ortega-Farias, S., Demarty, J., Wigneron, J.-P., Braud, I., Jacob, F., Lecharpentier, P., Otlé, C., Calvet, J.-C., Brisson, N. Future directions for advanced evapotranspiration modeling: assimilation of remote sensing data into crop simulation models and SVAT models. *Irrigation Drainage Syst.*, in press.
- Owen, P.C., 1968. A measuring scale for areas of cereals leaves. *Exp. Agric.* 4, 275–278.
- Pellenq, J., Boulet, G., 2004. A methodology to test the pertinence of remote-sensing data assimilation into vegetation models for water and energy exchange at the land surface. *Agronomie* 24, 197–204.
- Penman, H.L., 1948. Natural evaporation from open water, bare soil and grass. *Proc. R. Soc. Lond. A* 193, 120–146.
- Privette, J.L., Fowler, C., Wick, G.A., Baldwin, D., Emery, W.J., 1995. Effects of orbital drift on AVHRR products: normalized difference vegetation index and sea surface temperature. *Remote Sens. Environ.* 53, 164–177.
- Rahman, H., 1996. Atmospheric optical depth and water vapour effects on the angular characteristics of surface reflectance in NOAA AVHRR. *Int. J. Remote Sens.* 17 (15), 2981–2999.
- Rao, C.R.N., Chen, J., 1999. Revised post-launch calibration of the visible and near-infrared channels of the advanced very high resolution radiometer (AVHRR) on the NOAA-14 spacecraft. *Int. J. Remote Sens.* 20, 3485–3491.
- Ray, S.S., Dadhwal, V.K., 2001. Estimation of crop evapotranspiration of irrigation command area using remote sensing and GIS. *Agric. Water Manage.* 49, 239–249.
- Richardson, A.J., Wiegand, C.L., Wanjura, D.F., Dusek, D., Steiner, J.L., 1992. Multisite analyses of spectral-biophysical data for sorghum. *Remote Sens. Environ.* 41, 71–82.
- Rouse, J.W., Haas, R.H., Schell, J.A., Deering, D.W., Harlan, J.C., 1974. Monitoring the vernal advancement and retrogradation of natural vegetation. NASA/GSFC, Type III, Final Report, Greenbelt, MD, pp. 1–371.
- Schmugge, T.J., Kustas, W.P., Ritchie, J.C., Jackson, T.J., Rango, A., 2002. Remote sensing in hydrology. *Adv. Water Resour.* 25 (8–12), 1367–1385.

- Van Niel, T.G., McVicar, T.R., 2004. Current and potential uses of optical remote sensing in rice-based irrigation systems: a review. *Aust. J. Agric. Res.* 55, 155–185.
- Verhoef, W., Bach, H., 2003. Remote sensing data assimilation using coupled radiative transfer models. *Phys. Chem. Earth A/B/C* 28 (1–3), 3–13.
- Walter, I.A., Allen, R.G., Elliott, R., Jensen, M.E., Itenfisu, D., Mecham, B., Howell, T.A., Snyder, S., Brown, P., Echings, S., Spofford, T., Hattendorf, M., Cuenca, R.H., Wright, J.L., Martin, D., 2000. ASCE's standardized reference evapotranspiration equation. In: *Proceedings of Fourth National Irrigation Symposium*, ASAE, Phoenix, AZ, USA, 14–16 November.
- Webb, E.K., Pearman, G.I., Leuning, R., 1980. Correction of flux measurements for density effects due to heat and water vapour transfer. *Q. J. R. Meteorol. Soc.* 106, 85–100.
- Weir, A.H., Bragg, P.L., Porter, J.R., Rayner, J.H., 1984. A winter wheat crop simulation model without water or nutrients limitations. *J. Agric. Sci.* 102, 371382.
- Weiss, M., Trouffleau, D., Baret, F., Chauki, H., Prevot, L., Olioso, A., Bruguier, N., Brisson, N., 2001. Coupling canopy functioning and radiative transfer models for remote sensing data assimilation. *Agric. For. Meteorol.* 108, 113–128.
- Wright, J.L., Allen, R.G., Howell, T.A., 2000. Conversion between evapotranspiration references and methods. In: *Proceedings of the Fourth National Irrigation Symposium*, ASAE, Phoenix, AZ, USA, 14–16 November.